A Method of Moments Approach for the Simulation of Truncated RIS

Adam Abazi*, Jean Cavillot*, Christophe Craeye*,
*ICTEAM institute, Université Catholique de Louvain, Louvain-La-Neuve, Belgium,
adam.abazi@uclouvain.be, jean.cavillot@uclouvain.be and christophe.craeye@uclouvain.be

***Abstract*—A Method of Moments (MoM) approach for truncated Reflective Intelligent Surface (RIS) is proposed. The response of the truncated RIS is obtained as the sum of a term that includes only the grounded slab and a term with the response of the metallization on the same slab. The first term is truncated to the dimensions of the finite RIS based on a Physical Optics (PO) approximation. This approach is validated analytically and numerically in the case of a finite metallic plate on the grounded substrate. Besides, an analysis methodology for RIS made of printed parallel strips is developed assuming a structure infinite in one direction and is validated using a full 3D MoM code for a RIS finite in both directions.**

***Index Terms*—Reflective Intelligent Surface (RIS), Method of Moments (MoM), specular reflection, array truncation.**

I. Introduction

Reconfigurable Intelligent Surfaces (RISs) have attracted a great deal of interest in recent years in the antennas and propagation community [1]. Thanks to their ability to create abnormal reflections in the desired directions, RISs are expected to be one of the key elements of smart environments for future development of communication systems [2],[3]. RISs can be designed using several methods. For example, anomalous reflectors can be designed with the sheet impedance concept [4]. However, when using metallic patches to implement the impedance, the results may diverge from those obtained with the homogenized impedance [4]. Also, homogenization is not always possible, for instance when the substrate is very thin. In this case, it is worth relying exclusively on full-wave methods such as the Method of Moments (MoM). This in principle addresses a wider category of RIS structures. Finallly, another design technique was proposed based on periodically spaced metallic strips with periodic lumped loads [5].

This work presents a full-wave methodology for accounting for specular reflection on a grounded dielectric slab in the analysis and design of a truncated RIS. The approach is based on a physical optics (PO) approximation whose validity holds for sufficiently large structures relative to wavelength, which is typically the case in the context of RISs. This approach is developed analytically and verified numerically using a previously validated in-house 3D MoM code [6], [7]. Then, a MoM-based analysis methodology for RIS consisting of printed parallel strips, infinite in one direction, is introduced. In this case, the physical structure of the RIS is directly incorporated into the solver, rather than relying on a sheet impedance model. This approach eliminates the need to transition from the ideal impedance to the actual patch-implemented RIS, thereby enhancing the solver's reliability and widening the range of possible structures. This methodology is validated using a RIS that is finite in both dimensions, simulated with a full 3D MoM code. The paper is structured as follows. Section II presents the full-wave formulation giving the response of a truncated RIS accounting for the specular reflection and validates the model using a fully metallized example. Section III describes the MoM formulation for analyzing RIS made of infinite printed parallel strips and Section IV compares the results obtained from the developed formulation with those from a full 3D MoM code simulating a RIS composed of strips finite in both dimensions. Finally, conclusions are drawn in Section V.

II. Full-wave model for the response of a truncated RIS

This section describes the response of a truncated RIS in which the total deflected field is expressed as the sum of a term due only to the specular reflection of the finite grounded substrate and a term due to the radiation of MoM currents generated by an incident plane wave. The following subsections provide a detailed description of this approach and a validation through a full metallization example. This will be done for the TE incidence; the methodology is the same for the TM case. A schematic representation of the specular reflection term $\mathbf{F_s}$ and the radiation of the surface metal $\mathbf{F_m}$ is provided in Fig. 1.

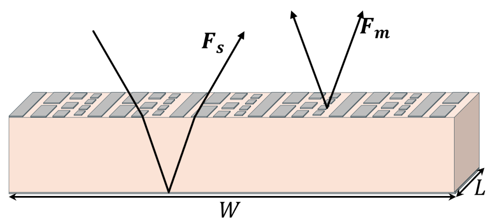

Fig. 1. Schematic representation of the specular reflection $\mathbf{F_s}$ and the radiation of the surface metal $\mathbf{F_m}$

A. Specular Reflection formulation

The analytical expression for specular reflection is reminded for a finite grounded dielectric slab in the absence of metallization on top of it. To account for truncation, it is assumed that the field pattern reflected by the grounded substrate can be modeled as the radiation of twice the magnetic currents $\mathbf{M}$, located on top of the grounded substrate of surface S, which corresponds to the RIS area (PO approximation). The corresponding radiation pattern, $\mathbf{F_s}$, is given by:

$$\mathbf{F_s}(\hat{\mathbf{u}}) = \frac{-jk_0\eta_0}{4\pi} \iint (-2\hat{\mathbf{u}} \times \mathbf{M}) e^{jk_0 \bar{\boldsymbol{\rho}} \cdot \hat{\mathbf{u}}} \, dS, \tag{1}$$

where k_0 is the free-space wavenumber, η_0 is the vacuum impedance, $\bar{\boldsymbol{\rho}}$ is the position vector to any point on the RIS surface and $\hat{\mathbf{u}} = (k_x^s, k_y^s, k_z^s)/k_0$ is the unit vector in the direction of observation. Assuming a TE-polarized incident wave, this expression can be rewritten using the relationship between the equivalent magnetic currents and the reflected electric field, $\mathbf{M} = -\hat{\mathbf{n}} \times \mathbf{E}_{TE}^s$, where $\hat{\mathbf{n}}$ is the unit vector normal to the surface and $\mathbf{E}_{TE}^s$ the TE-polarized reflected electric field:

$$\mathbf{F_s}(\hat{\mathbf{u}}) = \frac{jk_0\eta_0}{2\pi} \iint (\hat{\mathbf{u}} \times (-\hat{\mathbf{n}} \times \mathbf{E}_{TE}^s)) e^{jk_0 \bar{\boldsymbol{\rho}} \cdot \hat{\mathbf{u}}} \, dS. \tag{2}$$

In Eq. (2), $\mathbf{E}_{TE}^s$ can be expressed as a reflection coefficient Γ_{TE} multiplying the electric field $\mathbf{E}_{TE}^i$ of a TE-polarized incident plane wave on the surface [8]: $\mathbf{E}_{TE}^s = \mathbf{E}_{TE}^i \Gamma_{TE}$. The incident electric field can be further expressed as: $\mathbf{E}_{TE}^i = E_{TE}^i e^{-j(k_x^i x + k_y^i y)}(-\hat{y})$ where E_{TE}^i is the amplitude of the field and k_x^i and k_y^i are the x and y components of the incident wave vector. Expanding Eq. (2) yields the following closed-form expression for the reflection from the grounded dielectric substrate where the ground is assumed to be rectangular with dimensions $W \times L$:

$$\mathbf{F_s}(\hat{\mathbf{u}}) = \frac{-jk_0\eta_0}{2\pi} \cos\theta^s E_{TE}^i \Gamma_{TE}$$
$$W \mathrm{sinc}\left((k_x^i - k_x^s)\frac{W}{2}\right) L \mathrm{sinc}\left((k_y^i - k_y^s)\frac{L}{2}\right), \tag{3}$$

In this expression, θ^s is the angle of the scattering direction such that $\cos\theta^s = k_z^s/k_0$, k_x^s and k_y^s are the x and y components of the scattered wave vector, and W and L are the dimensions of the truncated RIS in the x and y directions, respectively. In Equation (3), the effect of truncation is evident through the appearance of factors that vary as cardinal sines, while the influence of the substrate's thickness and permittivity is captured in the reflection coefficient.

The PO approximation is found acceptable because the studied structure is invariant along horizontal coordinates and large compared to the wavelength.

B. Metallization response

The response of the RIS metallization can be expressed as the radiation of electric currents $\mathbf{J}$ induced on the metal by an incident wave in the presence of the grounded substrate. These currents can be computed using an in-house MoM solver [6]. Here, an expression of the radiated pattern, $\mathbf{F}_m$, due to the currents $\mathbf{J}$, is developed. An expression equivalent to Eq. (2) is obtained with $\mathbf{E}_{TE}^s$ replaced by $\mathbf{E}(\mathbf{J})$, the electric field induced by the MoM currents. This yields:

$$\mathbf{F_m}(\hat{\mathbf{u}}) = \frac{-jk_0\eta_0}{2\pi} \hat{\mathbf{u}} \times \hat{\mathbf{n}} \times [\underline{\underline{\tilde{G}}}(k_x^s, k_y^s) \tilde{\mathbf{J}}(k_x^s, k_y^s)] \tag{4}$$

where $\underline{\underline{\tilde{G}}}(k_x^s, k_y^s)$ is the Fourier transform of the dyadic layered media Green's function [8] and $\tilde{\mathbf{J}}(k_x^s, k_y^s)$ is the Fourier transform of the MoM currents. Assuming once again a TE configuration, the following holds:

$$\tilde{G}(k_x^s, k_y^s) = -\eta_0(1 + \Gamma_{TE}) \frac{1}{2\cos\theta^i}. \tag{5}$$

Moreover, the Fourier Transform of the currents can be analytically calculated by: $\tilde{\mathbf{J}}(k_x^s, k_y^s) = \mathbf{J_0} W \mathrm{sinc}((k_x^i - k_x^s)\frac{W}{2}) L \mathrm{sinc}((k_y^i - k_y^s)\frac{L}{2})$. Considering the specific case of a finite metallic plate on a grounded substrate, the PO approximation can be applied such that $\mathbf{J_0} \approx 2E_{TE}^i \cos\theta^i/\eta_0(-\hat{y})$. As a result, an approximate expression for $\mathbf{F_m}$, after development, is given by:

$$\mathbf{F_m}(\hat{\mathbf{u}}) = \frac{jk_0\eta_0}{2\pi} \cos\theta^s E_{TE}^i (1 + \Gamma_{TE})$$
$$W \ \mathrm{sinc}\left((k_x^i - k_x^s)\frac{W}{2}\right) L \ \mathrm{sinc}\left((k_y^i - k_y^s)\frac{L}{2}\right). \tag{6}$$

This analytical form for a fully metallic plate is used in the following section to validate the specular reflection model.

C. Full metallization validation

The proposed model is validated by considering a continuous PEC (perfect electric conductor) metallization on top of the grounded substrate. In this case, an analytical expression for the total radiation, i.e., the sum of $\mathbf{F_m}$ and $\mathbf{F_s}$, can be derived.

This expression is straightforwardly obtained by assuming total reflection on the PEC sheet, which translates into setting $\Gamma_{TE} = -1$ in Eq. (3):

$$\mathbf{F_{pec}}(\hat{\mathbf{u}}) = \frac{jk_0\eta_0}{2\pi} \cos\theta^s E_{TE}^i$$
$$W \mathrm{sinc}\left((k_x^i - k_x^s)\frac{W}{2}\right) L \mathrm{sinc}\left((k_y^i - k_y^s)\frac{L}{2}\right). \tag{7}$$

For the model to be correct, the equality $\mathbf{F_m} + \mathbf{F_s} = \mathbf{F_{pec}}$ must hold. By factoring out the common terms, this relation simplifies to:

$$(1 + \Gamma_{TE}) - \Gamma_{TE} = 1, \tag{8}$$

which is trivially satisfied.

The accuracy of this relation can also be verified numerically. A MoM code can be used to compute $\mathbf{F_m}$, while the analytical expressions are employed to calculate $\mathbf{F_s}$ and $\mathbf{F_{pec}}$. Additionally, the relation can be confirmed by using the MoM code to directly compute $\mathbf{F_{pec}}$ for a PEC sheet of same dimensions in free space, ensuring consistency between the analytical and numerical results. Fig. 2 shows the comparison of the different terms for a normally incident TE-polarized plane wave and scattering in directions given by θ^s. It can be seen that the sum of $\mathbf{F_m}$ and $\mathbf{F_s}$ closely approximates $\mathbf{F_{pec}}$, particularly at lower angles, where the amplitudes are nearly identical. Also, while the MoM-computed $\mathbf{F_{pec}}$ slightly diverges from the analytical result at higher angles, it retains a similar overall shape. Additionally, the amplitude of $\mathbf{F_s}$ is nearly equal to that of $\mathbf{F_{pec}}$, which is consistent with the fact that the main difference is the use of a physical-optics approximation in the case of $\mathbf{F_s}$.

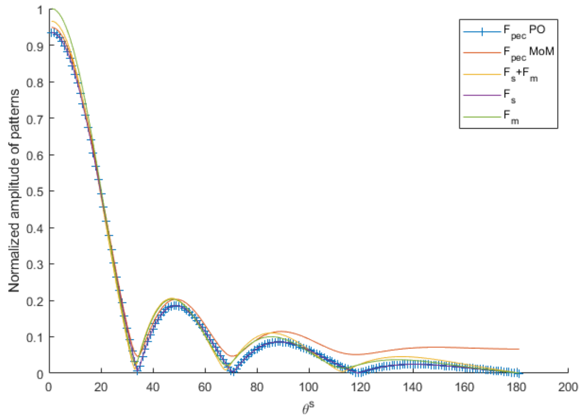

Fig. 2. Normalized amplitude of the patterns $\mathbf{F_m}$, $\mathbf{F_s}$, $\mathbf{F_{pec}}$ and $\mathbf{F_s} + \mathbf{F_m}$ - $\mathbf{F_{pec}}$ computed numerically (F_{pec} MoM) and analytically (F_{pec} PO)

III. Method of Moments formulation for a RIS made of printed parallel strips

The MoM model is developed for printed parallel strips positioned on a grounded substrate, as shown in Fig. 3. A Cartesian system of coordinates is defined such that the strips are infinite along the $\hat{y}$-axis, while their width W_b lies along the $\hat{x}$-axis.

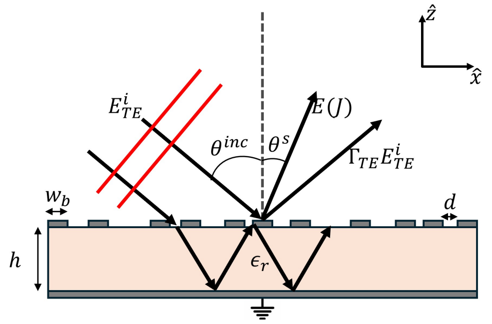

Fig. 3. Schematic illustration of the RIS configuration considered to develop the MoM model

The MoM formulation is obtained by applying Galerkin testing to the equation imposing zero total electric field on the conductors:

$$\int \mathbf{E^{exc}_{TE}} J_t^* \, dx + \int \mathbf{E}(\mathbf{J}) J_t^* \, dx = 0 \tag{9}$$

where $\mathbf{E^{exc}_{TE}}$ is the excitation field of the MoM given by $(1 + \Gamma_{TE})\mathbf{E^i_{TE}}$ and J_t^* is the complex conjugate of the testing function.

The excitation vector of the MoM, $\mathbf{V}$, arises from the first term by considering an incident TE plane wave, with phase dependence only along the x direction. This yields:

$$-\mathbf{V} = (1 + \Gamma_{TE}) E^i_{TE} \, e^{-jk_x x_{i,m}} \, w_i \, \text{sinc}\left(-k_x \frac{w_i}{2}\right) \tag{10}$$

where $x_{i,m}$ and w_i are the position of the center and the width of the i-th testing function.

The interaction term of the MoM, $\underline{\underline{\mathbf{Z}}}$, is derived from the second term in Eq. (9) and can be derived using the Fourier transform $\tilde{G}$ of the Green's function:

$$\underline{\underline{\mathbf{Z}}} = \frac{1}{2\pi} w_i w_j \int_{k_x} \tilde{G}(k_x) \, \text{sinc}\left(-k_x \frac{w_i}{2}\right) \text{sinc}\left(k_x \frac{w_j}{2}\right) \cdot e^{-jk_x(x_{i,m} - x_{j,m})} \, dk_x \tag{11}$$

where $x_{j,m}$ and w_j are the position of the center and the width of the j-th testing function. The domain of integration along k_x is strongly limited thanks to the extraction of an average-medium solution [9], for which the Green's function is known in space domain as $H_0^{(2)}(k_a R)/(4j)$ where $H_0^{(2)}(x)$ is the Hankel function of zero order and type 2 and k_a is the wavenumber in the medium of average permittivity between air and dielectric slab. For very small distances between basis and testing functions, the logarithmic singularity of that function is itself extracted and integrated analytically.

Additionally, using Eq. (5), the factors applied to obtain the radiation pattern can be linked to those of the excitation vector in Eq. (10), up to a constant factor of $-jk_0\eta_0/4\pi$. This relation allows for the definition of a matrix $\underline{\underline{\mathbf{\Omega}}}$, which has as many rows as strips and whose columns correspond to the excitation vector for each considered angle. Using this, the following equation can be formulated to give the bi-static pattern $\underline{\underline{\mathbf{F}}}_{RIS}(\theta^i, \theta^s)$:

$$\underline{\underline{\mathbf{F}}}_{RIS}(\theta^i, \theta^s) = \frac{-jk_0\eta_0}{4\pi} \underline{\underline{\mathbf{\Omega}}}^T \underline{\underline{\mathbf{Z}}}^{-1} \underline{\underline{\mathbf{\Omega}}} \tag{12}$$

where the superscript ^{T} denotes transposition.

IV. Validation

The MoM formulation introduced in Section III is validated using an in-house 3D MoM solver. To do so, currents are computed both with a code implementing the proposed formulation and with the in-house solver for a structure composed of 15 strips, each with a width of $\lambda/6$, arranged consecutively on a grounded dielectric slab of size $\lambda/15$ and relative permittivity $\epsilon_r = 2.5$ at a frequency of $5.8GHz$. For the 3D MoM solver, the strips are truncated to a length of 10λ, creating a finite structure in two dimensions. The excitation used to compute these currents is a TE plane wave with a positive $45°$ incidence angle. The patterns computed using these current are shown in Fig.4.

As seen in the figure, the two patterns exhibit the same overall shape and oscillations. The larger amplitude of the pattern computed from the structure finite in both directions can be attributed to the truncation along the y direction, which induces strong resonances in the strip currents, resulting in higher current amplitudes.

An example of anomalous reflection is shown in Fig. 5, obtained using both the 1D MoM formulation presented in Section III and the in-house 3D MoM solver. The structure

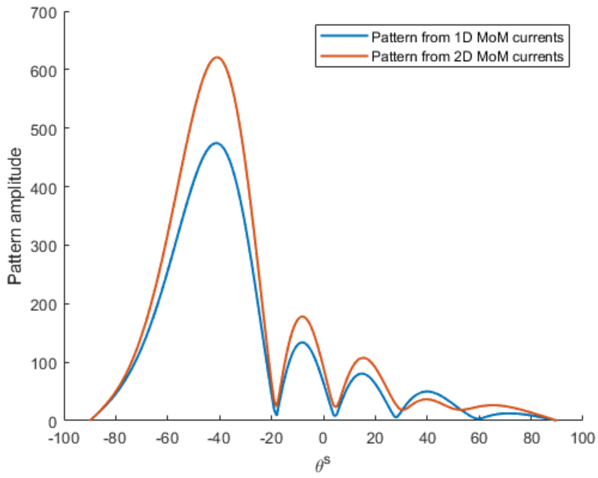

Fig. 4. Radiation patterns computed from 1D MoM currents and 2D MoM currents

consists of 15 strips separated by 0.75λ, and is excited by a TE plane wave incident at an angle of $45°$. The patterns exhibit the expected specular reflection at $-45°$ as well as a high amplitude corresponding to an anomalous reflection at $29°$. Once again, the results from both solvers show similar overall shapes, with the finite structure producing a larger amplitude, likely due to strong resonances in the strip currents. It is worth noting that the simulation time for this structure using the proposed 1D MoM formulation is 0.167 seconds on a conventional desktop computer.

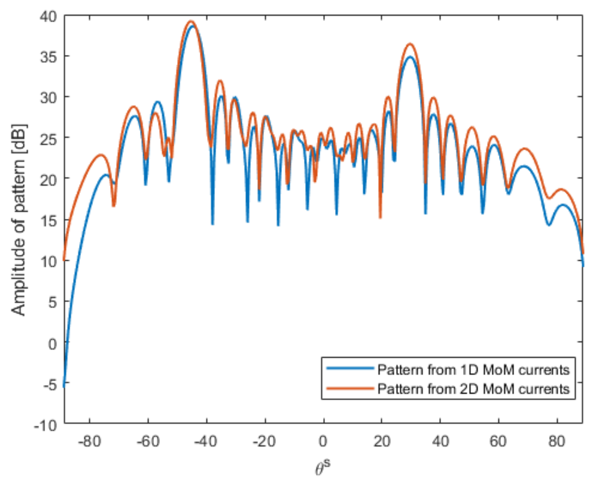

Fig. 5. Anomalous reflection at 29° for an incoming wave at 45°

V. Conclusion

A methodology was introduced for accounting for specular reflection in truncated RISs; the response of the finite grounded slab is computed based on a Physical Optical approach. This method was validated both analytically and numerically by considering a finite metal plate on a grounded dielectric substrate. Additionally, an analysis method for RIS composed of strips, infinite in one direction, was presented. This formulation was validated through numerical comparison with a structure finite in both dimensions, simulated using an in-house 3D MoM solver.

Acknowledgment

This study was conducted as part of the project Win2Wal2023/1 - N°2310026 - RAFINE, funded by SPW-Economie Emploi Recherche of Région wallonne.

References

[1] M. Di Renzo, A. Zappone; M. Debbah; M. S. Alouini; C. Yuen; J. de Rosny, S. Tretyakov, "Smart radio environments empowered by reconfigurable intelligent surfaces: how it works, state of research, and the road ahead," in IEEE JSAC, vol. 38, no. 11, pp. 2450-2525, Nov. 2020.

[2] R. Flamini, D. De Donno, J. Gambini, F. Giuppi, C. Mazzucco, A. Milani, L. Resteghini, "Toward a heterogeneous smart electromagnetic environment for millimeter-wave communications: an idustrial viewpoint," in IEEE TAP, vol. 70, no. 10, pp. 8898-8910, Oct. 2022.

[3] F. Yang, D. Erricolo and A. Massa, "Guest editorial smart electromagnetic environment," in IEEE TAP, vol. 70, no. 10, pp. 8687-8690, Oct. 2022.

[4] C. Yepes, M. Faenzi, S. Maci, and E. Martini, "Perfect non-specular reflection with polarization control by using a locally passive metasurface sheet on a grounded dielectric slab", APL 118, 231601,2021

[5] Y. Li, X. Ma, X. Wang, G. Ptitcyn, M. Movahediqomi and S. A. Tretyakov, "All-angle scanning perfect anomalous reflection by using passive aperiodic gratings," in IEEE TAP, vol. 72, no. 1, pp. 877-889, Jan. 2024

[6] H. V. Bui, S. N. Jha and C. Craeye, "Fast Full-Wave Synthesis of Printed Antenna Arrays Including Mutual Coupling," in IEEE TAP, vol. 64, no. 12, pp. 5163-5171, Dec. 2016.

[7] J. Cavillot, M. Bodehou and C. Craeye, "Metasurface antennas design: full-wave feeder modeling and far-field optimization," in IEEE TAP, vol. 71, no. 1, pp. 39-49, Jan. 2023.

[8] N. K. Das and D. M. Pozar, "A generalized spectral-domain Green's function for multilayer dielectric substrates with application to multilayer transmission lines," in IEEE TMTT, vol. 35, no. 3, pp. 326-335, Mar 1987.

[9] Y. L. Chow, J. J. Yang, D. G. Fang and G. E. Howard, "A closed form spatial Green's function for the thick microstrip substrate," IEEE TMTT, vol. 39, no. 3, pp. 588-592, Mar. 1991.